# Focal Magnetic Stimulation of an Axon

Peter J. Basser

*Abstract*—**The induced electric field produced by a circular coil during magnetic stimulation of an axon is derived from Maxwell's equations. The foci and virtual cathodal and anodal regions are predicted as a function of coil radius and orientation. Two virtual anode and cathode pairs are predicted, one lying outside the coil's perimeter and predominant in the far field, and one lying within the perimeter of the coil which may stimulate the axon when the coil and nerve are in close proximity. When the coil is positioned tangent to the nerve, an orientation commonly used in clinical magnetic stimulation, the foci of the predominant cathode and anode pair are extremely sensitive to changes in coil placement. In addition, the radius of curvature of the activating function, a measure of the size of the virtual cathode at threshold, is predicted to decrease with decreasing coil diameter and distance to the nerve. These predictions may help explain observed variability in measurements of conduction velocity and latency during magnetic stimulation of peripheral axons.**

## I. Introduction

MAGNETIC stimulation is a method to noninvasively and painlessly excite nerves [1], [2] by electromagnetic induction. Yet, difficulty to predict, locate and localize the site of stimulation (virtual cathode) have been cited as disadvantages that limit its utility in routine peripheral nerve conduction studies [1]–[5]. These deficiencies are addressed with a mathematical model. The model is used to elucidate several sources of experimental error in measurements of latency and conduction velocity and to recommend ways to mitigate them. Errors may be geometric in origin. Here, the model is used to furnish estimates of changes in the distribution of the virtual anode(s) and cathode(s), with respect to changes in geometry and orientation of the coil and axon. Other errors may be attributed to incomplete knowledge of the electric field distribution near the axon. Here, a closer examination of the field distribution near the coil reveals new regions of excitation and inactivation. Finally, a figure of merit for the localization of the cathodic region is proposed whose dependence on coil diameter and geometry is predicted.

## II. The Activating Function for *In Vitro* Magnetic Stimulation of a Myelinated Axon

Applied electric fields caused by electromagnetic induction or charge may depolarize or hyperpolarize nerves by producing transmembrane currents. In mathematical models of nerve stimulation, electric fields caused by current injection or by extracellular electrodes appear as a source of transmembrane potential in the cable equation of an axon [6], [7], a term which Rattay has called the activating function. It is the input to the cable equation whose output is the axon's transmembrane potential distribution. As such, it relates variables under experimental control to a dependent variable that we wish to predict in nerve stimulation. It was only recently that magnetic stimulation was explained within this framework and its activating function, $-\partial\varepsilon_y(y,t)/\partial y$, was derived (where $\varepsilon_y(y,t)$ is the net applied electric field in the axial direction of the nerve fiber) [8]–[10]. An analytic or closed-form expression for this quantity is derived using Maxwell's equations.

Fig. 1 shows a circular stimulating coil lying above an axon in a uniform volume conductor. When the coil is in a plane parallel to the bath surface, the induced surface charge distribution at the air/bath interface is zero [11]. The activating function, which equals the gradient of the component of the net electric field along the axis of the axon, is given by [8]

$$-\frac{\partial\varepsilon_y(x_0,y,-z_0,t)}{\partial y}=\frac{\partial}{\partial y}\frac{\partial A_y(x_0,y,-z_0,t)}{\partial t}. \tag{1}$$

In (1), $A_y$ is the component of the magnetic vector potential parallel to the axis of the axon, $x_0$ is the distance between the axon and the axis of the coil, and $z_0$ is the distance between the axon and the plane of the coil.

The magnetic vector potential, $\mathbf{A}(\mathbf{r})$ at position $\mathbf{r}$, caused by a current density, $\mathbf{J}(\mathbf{r})$, is given by

$$\mathbf{A}(\mathbf{r})=\frac{\mu}{4\pi}\int\frac{\mathbf{J}(\mathbf{r}\prime)}{|\mathbf{r}-\mathbf{r}'|}\mathrm{d}r'^3 \tag{2}$$

where $\mu$ is the permeability of free space. For a current $I(t)$ flowing in a circular coil, only the azimuthal component of $\mathbf{A}$, $A_\phi$, is nonvanishing. It can be written as a line integral in spherical coordinates, e.g., [12]

$$A_\phi(\rho,\theta,t)=I(t)\frac{\rho_c\mu}{\pi}\int_0^{2\pi}\frac{\cos\phi' d\phi'}{\sqrt{\rho_c^2+\rho^2-2\ \rho_c\rho\sin\theta\cos\phi'}} \tag{3}$$

where $\rho_c$ is the radius of the coil. This expression simplifies to [12]

$$A_\phi(\rho,\theta,t)=I(t)\frac{\rho_c\mu}{\pi\sqrt{\rho_c^2+\rho^2+2\ \rho_c\rho\sin\theta}}\times\left(\frac{2}{k^2}(K(k)-E(k))-K(k)\right). \tag{4}$$

Above, $E(k)$ and $K(k)$ are complete elliptic integrals of the first and second kinds [12], [13] and

$$k^2(\rho,\theta)=\frac{4\ \rho_c\rho\sin\theta}{\rho_c^2+\rho^2+2\ \rho_c\rho\sin\theta}. \tag{5}$$

Manuscript received May 7, 1991; revised August 19, 1992 and January 25, 1994.

The author is with the Biomedical Engineering and Instrumentation Program, National Center of Research Resources, National Institutes of Health, Bethesda, MD 20892 USA.

IEEE Log Number 9401321.

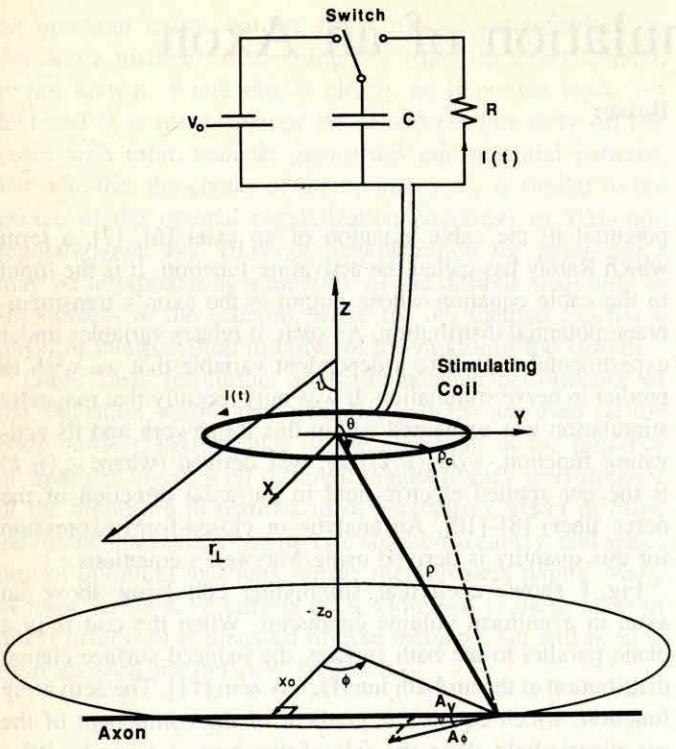


Fig. 1. The current source, stimulating coil and myelinated axon in an *in vitro* experiment. The axon is parallel to the $y$-axis; it lies $z_0$ below the coil and $x_0$ from its axis. When the capacitor is discharged, the current, $I(t)$ in the coil induces an electric field in the tissue bath whose gradient in the direction of the nerve axis is the activating function. It determines the local transmembrane current in the axon and is related to the magnetic vector potential, $A_\phi$, and its component lying along the axon, $A_y$ by (6).

Referring to Fig. 1, $A_y$ is simply the component of $A_\phi$ along the nerve axis

$$A_y = A_\phi \cos\phi. \tag{6}$$

Therefore, the activating function for magnetic stimulation can be written as an analytic expression

$$\frac{\partial}{\partial t}\left(\frac{\partial A_y}{\partial y}\right) = \frac{dI(t)}{dt}\frac{\partial}{\partial y}\left(\frac{\rho_c \mu \cos\phi}{\pi\sqrt{\rho_c^2+\rho^2+2\,\rho_c\rho\sin\theta}} \times \left(\frac{2}{k^2}(K(k)-E(k))-K(k)\right)\right) \tag{7}$$

The following identities [13], [14]

$$\frac{dK(k)}{dk} = \frac{E(k)}{k(1-k^2)} - \frac{K(k)}{k} \tag{8a}$$

and

$$\frac{dE(k)}{dk} = \frac{E(k)-K(k)}{k}, \tag{8b}$$

the chain rule, and the transformation rules from spherical to Cartesian coordinates,

$$\rho(x_0, y, -z_0) = \sqrt{x_0^2+y^2+z_0^2} \tag{9a}$$

$$\phi(x_0, y, -z_0) = \tan^{-1}\left(\frac{x_0}{y}\right) \tag{9b}$$

$$\theta(x_0, y, -z_0) = \cos^{-1}\left(\frac{-z_0}{\sqrt{x_0^2+y^2+z_0^2}}\right) \tag{9c}$$

can be used to write the activating function in closed-form in terms of $x_0$, $y$ and $z_0$. It is represented symbolically as

$$-\frac{\partial \varepsilon_y(x_0, y, -z_0, t)}{\partial y} = \frac{\partial}{\partial t}\left(\frac{\partial A_y(x_0, y, -z_0, t)}{\partial y}\right) = \frac{dI(t)}{dt} f(x_0, y, -z_0) \tag{10}$$

where $f$ is a function that is too lengthy to include here.

The electric field components in the $x$ and $y$ directions, $\varepsilon_x$ and $\varepsilon_y$, are unchanged when we relax the assumption of uniformity of the conductive medium provided that its electrical properties are only inhomogeneous in $z$ [15]. Therefore, the activating function in (10) is also valid for tissue-like materials, including layered media whose electrical properties may be discrete functions of $z$.

There is a tacit assumption that the axon is infinite in this study. However, as long as the nerve terminates more than a few coil radii from the center of the coil, the effect of the termination can generally be ignored because the electric field and its gradient there are negligible. A suggestion for treating this problem is contained in Basser and Roth [16].

Typically, for magnetic stimulation the characteristic length of the applied electric field is much greater than the space constant of the axon [16]. If the stimulus is below threshold, then the spatial distribution of the activating function, $f$, and the transmembrane potential that it produces are qualitatively similar [8], [16]. In particular, their extrema occur at the same points along the axon—a results, that follows from dimensional analysis of the cable equation of magnetic stimulation [16]. Since (10) is a separable function of space and time, $dI/dt$ only modulates the amplitude of $f$ but does not alter its spatial distribution, in particular, the location of its extreme values. Therefore, the loci and extent of the cathodic and anodic regions produced by the activating function can be revealed by analyzing $f$ alone.

## III. Properties of $f$, the Space Dependent Part of the Activating Function

The function $f$ depends only on the geometry of the coil and the nerve. It is plotted in Fig. 2(a) and (b) as a function of the normalized axial distance along a nerve, $y/\rho_c$, at two different distances between the coil axis and the nerve. Fig. 2(a) shows $f$ for $x_0 = 1.5\ \rho_c$ and $z_0 = 0.1\ \rho_c$, a region outside the coil's perimeter and just below the plane of the coil. There is only one maximum and one minimum corresponding to the focus of the virtual anode and cathode. Fig. 2(b) shows $f$ for $x_0 = 0.5\ \rho_c$ and $z_0 = 0.1\ \rho_c$, a region within the perimeter of the coil and just below it. Besides the original anode and cathode pair, a new maximum and minimum appear. Since extrema in $f$ correspond to regions that are either maximally hyper- or depolarized, these points are the centers or foci of the anodal and cathodal regions. Therefore, the activating function depicted in Fig. 2(b) could potentially depolarize two distinct regions along the nerve. In both figures extrema are antisymmetric about $y = 0$, the plane perpendicular to the nerve passing through the center of the coil. Also depicted is $d$, defined as half the distance between the centers of the principal virtual cathode and anode.

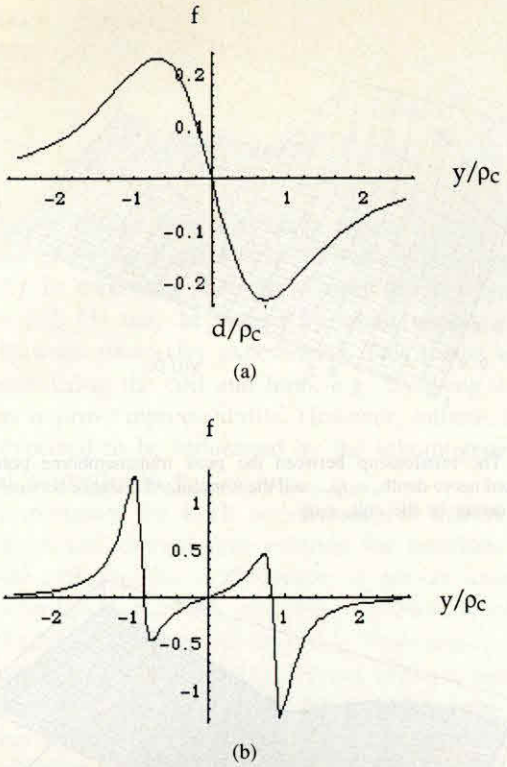


Fig. 2. The spatially varying part of the activating function, $f$, plotted against the normalized axial distance for $z_0 = 0.1\ \rho_c$ with (a) $x_0 = 1.5\ \rho_c$ and (b) $x_0 = 0.5\ \rho_c$. Extrema in transmembrane potential are antisymmetric about $y = 0$. Also shown is $d$, which is half the distance between principal extrema.

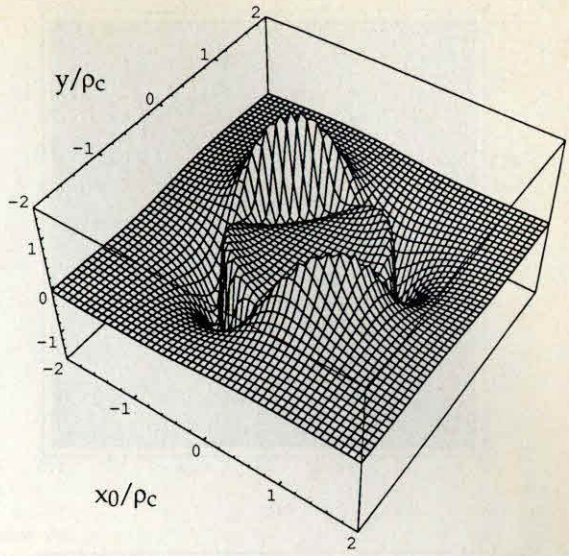


Fig. 3. The space dependent term in the activation function, $f$, plotted against $x_0/\rho_c$, the normalized distance between axon and coil and the normalized axial distance along the axon, $y/\rho_c$, at a particular depth, $z_0 = 0.1\ \rho_c$. Two distinct regions are seen. When $|x_0| \geq \rho_c$, the distance between extrema in $f$ increases as a function of $x_0$ and only one maximum and one minimum are seen. When $|x_0| \leq \rho_c$, the distance between extrema decreases with $x$ and two maxima and two minima are seen. These extrema correspond to regions of maximal membrane hyper- and depolarization.

Curves like the ones shown are assembled in Fig. 3 and shown as a 3-Dimensional plot of $f$ versus $x_0/\rho_c$, the normalized distance between nerve and coil and $y/\rho_c$, the normalized axial distance along the nerve, at depth $z_0 = 0.1\ \rho_c$. When $x_0 \geq \rho_c$, the distance between extrema increases slowly as a function of $x_0$. Again, only one maximum and one minimum in $f$ are seen. When $x_0 < \rho_c$, the distance between extrema decreases more rapidly with $x_0$; the secondary anode and cathode now appear. At $x = \rho_c$ and $y = 0$, the secondary anode and cathode coalesce, exactly cancelling each other.

Fig. 4 shows contour plots of $f$ against $x_0/\rho_c$ and $y/\rho_c$ for three different depths, a) $z_0 = 0.2\ \rho_c$, b) $z_0 = 0.2\ \rho_c$ and c) $z_0 = 0.5\ \rho_c$. Contours are all equally scaled with gray levels from black to white corresponding to values of $f$ between -2.5 and 2.5 $(\text{mV/cm}^2)/(\text{Amp}/\mu\text{s})$. In Fig. 4(a), the secondary anode and cathode that form in the interior of the coil are clearly seen. In Fig. 4(a), the secondary anode and cathode are already attenuated, and in Fig. 4(b) they no longer appear. The secondary anode and cathode appear only close to the coil.

This dichotomous behavior can be explained in the following way. Near the coil, the field that the nerve experiences is caused primarily by the curved wire segment lying just above it but skew to it. The secondary virtual anode and cathode pair is generated by this electric field, which decays with $\log(r)$. Farther from the coil, the field from the entire current loop is felt by the nerve which drops off with $1/r$. One must be mindful of this behavior when using a discrete approximation of the continuous stimulating coil to calculate the electric field distribution. Roth's 64-sided polygon approximation to a circular coil [11], [17], which accurately predicts the electric field far from the coil, is also expected to correctly predict it when the length of an edge is comparable to $z_0$. Other *ad hoc* methods, however, may not be successful in both regimes.

These extrema are highly ordered. In the far field, they are approximately collinear. They lie on the intersection of the planes $\phi_{\max} = \pm\pi/4$ (i.e., $y = \pm x_0$) and an inverted cone that passes through the stimulating coil whose subtended angle, $\upsilon$, is shown in Fig. 1. The ratio of $r_\perp - \rho_c$ and $z_0$, where $r_\perp$ is the distance between the $z$-axis and the cone's surface, is approximately -0.44. A plot of $(r_\perp - \rho_c)/\rho_c$ versus $z_0/\rho_c$ is shown in Fig. 5. Near the coil, the relationship diverges from linearity.

We can predict relationships between the magnitude of the activating function and coil geometry. Fig. 6 shows the peak in the activating function, $f_{\max}$, plotted against the normalized nerve depth, $z_0\ \rho_c$, and normalized distance between the nerve and the center of the coil, $x_0\ \rho_c$. One important result is that extrema in $f$ occur where the nerve is nearly tangent to, and lies just below, the coil, i.e., $x_0 \cong 0.76\ \rho_c$ and $|z_0| \ll \rho_c$. This may explain why this coil orientation is so efficacious in clinical magnetic stimulation [2], [3].

Fig. 7 shows the normalized displacement of a global extremum in the activating function from the $y$-axis, $d/\rho_c$, plotted against the normalized nerve depth, $z_0/\rho_c$, and the normalized distance between the nerve and the center of the coil, $x_0/\rho_c$. Far from the center of the coil, $d$ increases slowly with $x_0$ and $z_0$. But, for $x_0 \cong 0.76\ \rho_c$ and $|z_0| \ll \rho_c$, the coil orientation corresponding to maximal stimulation efficacy, $d$ is most sensitive to coil position, i.e., changes in $x_0$ and $z_0$!

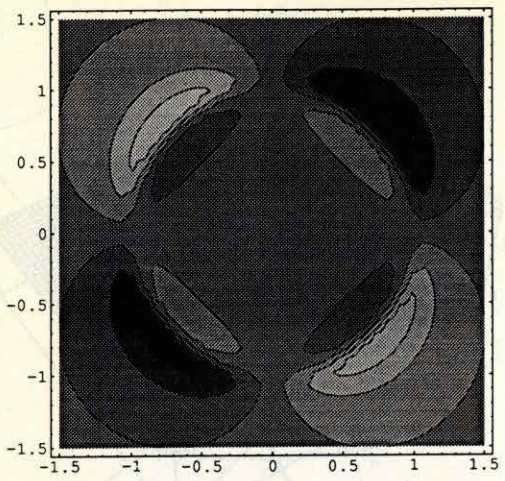


(a)

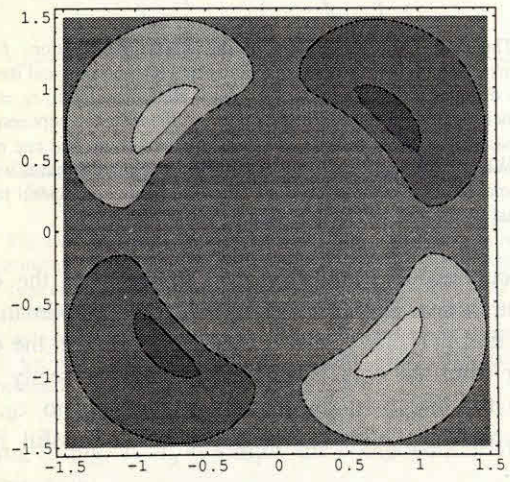


(b)

Fig. 4. Contour plots of the space dependent term in the activation function, $f$, plotted against $x_0/\rho_c$, the normalized distance between nerve and coil (horizontal axis), $y/\rho_c$, and the normalized axial distance along the nerve (vertical axis), at depths, (a) $z_0 = 0.2\ \rho_c$, and (b) $z_0 = 0.5\ \rho_c$. In these gray scale plots, black corresponds to $f = -2.5$ and white to $f = 2.5$.

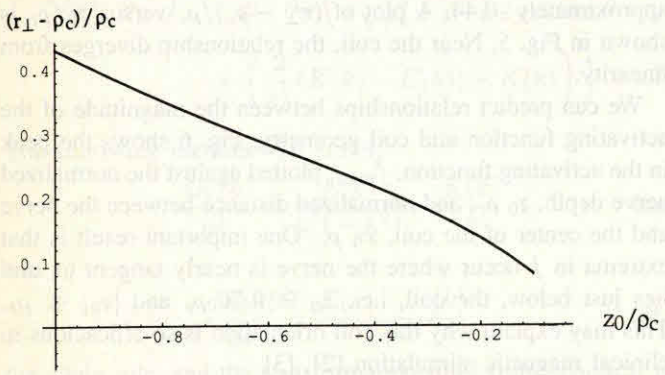


Fig. 5. The plot of $(r_\perp - \rho_c)/\rho_c$ versus $z_0/\rho_c$, where $r_\perp$ is the projection of the vector to the extremum in the plane of the coil.

## IV. Sources of Experimental Error

The previous two paragraphs suggest a trade-off between achieving maximal stimulus amplitude and being certain of the location of the foci of the virtual cathode and anode. To address this issue, the model can be used to furnish

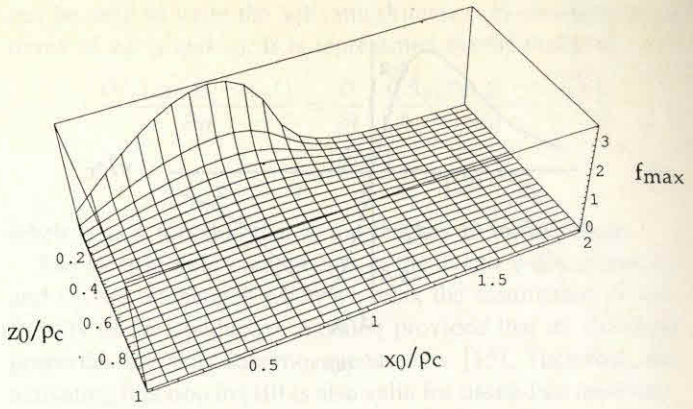


Fig. 6. The relationship between the peak transmembrane potential, the normalized nerve depth, $z_0/\rho_c$, and the normalized distance between the nerve and the center of the coil, $x_0/\rho_c$.

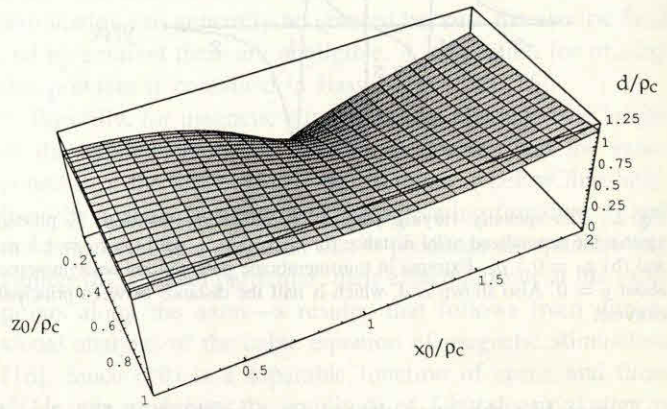


Fig. 7. The normalized distance between peaks in transmembrane potential, $d/\rho_c$, plotted against the normalized nerve depth, $z_0/\rho_c$, and the normalized distance between the nerve and the center of the coil, $x_0/\rho_c$. Marked differences exist between the locus displacements and depth for $x_0 \geq \rho_c$ and $x_0 < \rho_c$. Extrema correspond to regions of hyper- and depolarization.

sensitivities—estimates of changes in dependent variables with respect to changes in independent variables. First, we estimate the change in the location of the focus caused by changes in the depth of the nerve or its distance from the coil axis. When the coil is positioned tangent to the nerve, then a small displacement in $x_0$, $\delta x_0$, changes the position of the focus of the stimulating cathode and its distance to the anode, $2\ \delta d$. According to Fig. 7 for $x_0 \cong \rho_c$ and $|z_0| \ll \rho_c$, a variation in the distance of the nerve from the coil axis, $\delta x_0/\rho_c = 0.1$, causes a change in the distance between anode and cathode, $2 * \delta d/\rho_c = 2 * 0.2$, and a displacement of the cathode that is half that, $\delta d/\rho_c = 0.2$. For a coil with $\rho_c = 4.5$ cm, this displacement is $2 * \delta d \cong 1.8$ cm. The change in virtual electrode displacement with distance is given approximately as

$$2\frac{\delta d/\rho_c}{\delta x_0/\rho_c} = 4.0. \tag{11}$$

A variation in the distance of the nerve from the coil axis, $\delta z_0/\rho_c = 0.1$, also causes a change in the distance between anode and cathode, $2 * \delta d/\rho_c = 2 * 0.3$ and a displacement of the cathode, $\delta d/\rho_c = 0.3$. For a coil with $\rho_c = 4.5$ cm,

the distance between anode and cathode, $2 * \delta d \cong 2.4$ cm. The change in virtual electrode displacement with distance is approximately

$$2\frac{\delta d/\rho_c}{\delta z_0/\rho_c} = 6.0. \tag{12}$$

Thus a small change in coil position causes a proportionally larger change in the displacement between virtual electrodes. Variability in measuring their locus near the ulnar nerve in the wrist [2], [3] may be caused by small variations in $x_0$ and $z_0$ between successive experiments. This model suggests that immobilizing the coil and limb, e.g., by using a fixture [18], may improve reproducibility. However, cathode location is also expected to be influenced by the inhomogeneities of electrical properties in this region.

It was proposed by Roth and Basser [8] that reversing the sense of coil current also reverses the positions of the anode and cathode. So, a difference in arrival time of an action potential to a distant recording electrode is expected when clockwise and counterclockwise monophasic current pulses are used [8], [16]. The separation between anode and cathode can then be estimated by dividing this delay by the conduction velocity. Experiments to test this prediction have been performed [4], [5], [19]. Recent results of Nilsson *et al.* [4], [5] and Maccabbee *et al.* [20] support the existence of well separated, distinct anodal and cathodal regions in agreement with theory [8], [16]. In these experiments, nerve and coil orientation should be carefully controlled. Besides the previously discussed errors due to coil and nerve placements, there is an additional possible source of experimental error that should be controlled. If stimulus strength were great enough and $z_0$ were small enough, both cathodes could elicit an action potential. The (most distal) cathode closest to the recording electrode would appear to be the origin of the action potential. In close proximity to this cathode is the distal-most anode. When coil current is reversed, anodes and cathodes are reversed too, so the distal-most anode becomes the new origin of stimulation. Since the distal anode and cathode are near one another, e.g. 0.15 $\rho_c$, the latency difference would be reduced by as much as a factor of twenty.

Some problems of uncertainty and variability of cathode placement are expected to be mitigated with a coil shaped like a four-leafed clover. This design, proposed by Roth *et al.* [21], places the virtual cathode directly below its center. The locus of stimulation is not expected to migrate as the distance between coil and nerve changes.

## V. Increasing Stimulus Localization by Decreasing Stimulating Coil Diameter

Does decreasing the coil diameter decrease the size of the anodal and cathodal regions along the nerve? Cohen and Cuffin [22] and Yunokuchi and Cohen [23] have tried to achieve greater focal stimulation in magnetic stimulation of the brain by reducing coil diameter. Not surprisingly, intuition about the dependence of stimulus localization on coil size for stimulation of peripheral nerve can be gleaned from analysis of the activating function.

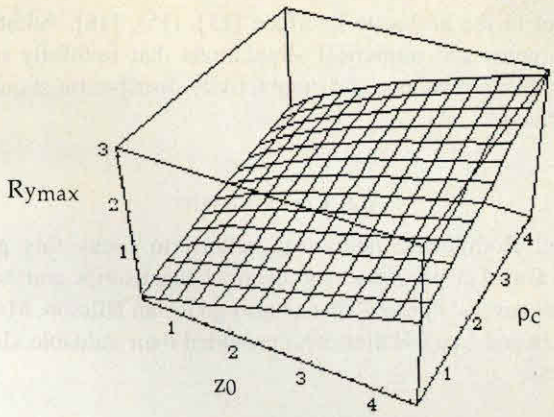


Fig. 8. The radius of curvature of the peak of the activating function, $Ry_{\max}$, as a function of the radius of the stimulating coil, $\rho_c$ and the nerve depth, $z_0$ for $x_0 > \rho_c$. The index falls off monotonically with the coil radius, indicating that greater focal stimulation may be achieved with decreases in coil diameter and distance to the nerve.

One measure of stimulus localization is the effective width of the cathode or anode near its peak. The radius of curvature of the normalized activating function in the neighborhood of an extremum is used as a relative measure of the extent of the cathode

$$R(y_{\max}) = \sqrt{\frac{f(x_0, y_{\max}, -z_0)}{\dfrac{\partial^2 f(x_0, y_{\max}, -z_0)}{\partial y^2}}}. \tag{13}$$

This quantity measures the effective width of the activating function near an extremum. Fig. 8 shows the relationship between $R(y_{\max})$, the radius of the stimulating coil, $\rho_c$, and the depth of the nerve, $z_0$. In constructing this figure, the nerve is assumed to lie tangent to the coil, $x_0 = \rho_c$, where the magnitude of stimulation is near its global optimum. The radius of curvature is a monotonically increasing function of depth and coil radius, indicating that greater focal stimulation is achieved by decreasing both coil diameter and the distance to the nerve.

## VI. Concluding Remarks

Analysis of an analytic expression of the activating function for magnetic stimulation has produced several experimentally testable predictions relating stimulus strength, the location and spatial extent of the virtual anode(s) and cathode(s), and the coil geometry and orientation with respect to the axon. Since there are no free parameters to adjust, these predictions are unambiguous.

This analysis can be extended to model other coil geometries by superposition of activating functions. For example, one could superpose the fields caused by individual wire loops to model a butterfly [24], four-leaf clover [21] or a coil with multiple windings of wire.

These results may not be quantitative for magnetic stimulation when the radius of curvature of the air/volume conductor interface is commensurate to the radius of the coil [11], [16], when inhomogeneities of electrical properties are not only a function of depth [15] or the orientation of the coil is not

parallel to the air/tissue interface [11], [15], [16]. Additional experiments and numerical simulations that faithfully incorporate tissue anatomy and conductivity distribution should be performed.

## ACKNOWLEDGMENT

Brad Roth made many suggestions to focus this paper. Priya Gopalan proofread the original manuscript and helped prepare several figures. Thanks also go to Jan Nilsson, Marcela Panizza and Mark Hallett who provided their valuable clinical expertise.

## REFERENCES

[1] M. Hallett and L. G. Cohen, "Magnetism: a new method for stimulation of nerve and brain," *JAMA*, vol. 262, pp. 538–541, 1989.
[2] B. A. Evans, W. J. Litchy and J. R. Daube, "The utility of magnetic stimulation for routine peripheral nerve conduction studies," *Muscle & Nerve*, vol. 11, pp. 1074–1078, 1988.
[3] B. A. Evans, "Magnetic stimulation of the peripheral nervous system," *J. Clin. Neurophys.*, vol. 8, pp. 77–84, 1991.
[4] J. Nilsson, M. B. Panizza, B. J. Roth, P. J. Basser, L. G. Cohen, G. Caruso and M. Hallett, "Cathode identification in magnetic stimulation of a peripheral nerve: Mathematical modelling supported by findings in normal volunteers," in *Proc. 43rd Annu. Meeting of the American Academy of Neurology*, Boston, MA, 1991.
[5] J. Nilsson, M. Panizza, B. J. Roth, P. J. Basser, L. G. Cohen, G. Caruso and M. Hallett, "Determining the site of stimulation during magnetic stimulation of a peripheral nerve," *Electroenceph. clin. Neurophysiol.*, vol. 85, pp. 253–264, 1992.
[6] J. L. Davis and R. L. deNó, "Contribution to the mathematical theory of the electrotonus," *Rock. Inst. Mon.*, vol. 131, pp. 442–496, 1947.
[7] F. Rattay, "Analysis of models for external stimulation of axons," *IEEE Trans. Biomed. Eng.*, vol. BME-33, pp. 974–977, 1986.
[8] B. J. Roth and P. J. Basser, "A model of the stimulation of a nerve fiber by electromagnetic induction," *IEEE Trans. Biomed. Eng.*, vol. 37, pp. 588–597, 1990.
[9] P. J. Basser and B. J. Roth, "Electromagnetic stimulation of a myelinated axon," in *Proc. 16th Annu. Northeast Bioeng. Conf.*, Penn. State Univ., 1990, pp. 129–130.
[10] P. J. Basser, R. S. Wijesinghe and B. J. Roth, "The activating function for magnetic stimulation derived from a three-dimensional volume conductor model," *IEEE Trans. Biomed. Eng.*, vol. 39, pp. 1207–1210, 1992.
[11] B. J. Roth, L. G. Cohen, M. Hallett, W. Friauf and P. J. Basser, "A theoretical calculation of the electric field induced by magnetic stimulation of a peripheral nerve," *Muscle & Nerve*, vol. 13, pp. 734–741, 1990.
[12] J. D. Jackson, *Classical Electrodynamics*, New York: John Wiley & Sons, 1975.
[13] P. F. Byrd and M. D. Friedman, *Handbook of Elliptic Integrals for Engineers and Scientists*, Springer-Verlag, 1971.
[14] W. R. Smythe, *Static and Dynamic Electricity*, McGraw-Hill, 1968.
[15] K. P. Esselle and M. A. Stuchly, "Neural stimulation with magnetic fields: analysis of induced electric fields," *IEEE Trans. Biomed. Eng.*, vol. 39, pp. 693–700, 1992.
[16] P. J. Basser and B. J. Roth, "Stimulation of a myelinated nerve axon by electromagnetic induction," *Med. & Biol. Eng. & Comput.*, vol. 29, pp. 261–268, 1991.
[17] L. G. Cohen, B. J. Roth, J. Nilsson, N. Dang, M. Panizza, S. Bandinelli, W. Friauf and M. Hallett, "Effects of coil design on delivery of focal magnetic stimulation, Technical considerations," *Electroenceph. Clin. Neurophysiol.*, vol. 75, pp. 350–357, 1990.
[18] M. Traad, "A quantitative positioning device for transcranial magnetic stimulation," in *Proc. 11th Annu. Int. Conf. IEEE EMBS*, Philadelphia, PA, 1990, p. 2246.
[19] P. J. Maccabbee, V. E. Amassian, R. Q. Cracco, L. Eberle, A. Rudell and K. S. Lai, "Effective anode and cathode are very close together when stimulating peripheral nerve with the magnetic coil," in *Proc. 20th Annu. Meeting of the Society for Neurosci.*, St. Louis, MO, 1990, p. 1261.
[20] P. J. Maccabbee, V. E. Amassian, L. Eberle and R. Q. Cracco, "Magnetic stimulation of straight and bent amphibian and mammalian peripheral nerve *in vitro:* Locus of excitation," *J. Physiol. (Lond.)*, vol. 460, pp. 201–219, 1993.
[21] B. J. Roth, P. J. Maccabbee, L. Eberle, V. E. Amassian, M. Hallett, J. Cadwell, G. D. Anselmi and G. T. Tatarian, "*In vitro* evaluation of a four-leaf coil design for magnetic stimulation of peripheral nerve," *Electroenceph. clin. Neurophysiol.*, vol. 93, pp. 68–74, 1994.
[22] D. Cohen and B. N. Cuffin, "Developing a more focal magnetic stimulator, Part I: Some basic principles," *J. Clin. Neurophys.*, vol. 8, pp. 102–111, 1991.
[23] K. Yunokuchi and D. Cohen, "Developing a more focal magnetic stimulator. Part II: Fabricating coils and measuring induced current distributions," *J. Clin. Neurophys.*, vol. 8, pp. 112–120, 1991.
[24] S. Ueno, K. Harada, C. Ji and Y. Oomura, "Magnetic nerve stimulation without interlinkage between nerve and magnetic flux," *IEEE Trans. Mag.*, vol. MAG-20, pp. 1660–1662, 1984.

**Peter J. Basser** received the A.B. degree in engineering sciences from Harvard College in 1980 and the S.M. and Ph.D. degrees from Harvard University in 1982 and 1986, respectively.

He is currently a Biomedical Engineer in the Biomedical Engineering and Instrumentation Program, National Institutes of Health. His primary research interests include characterizing transport and electromechanochemical conversion in biological tissue and polymer gels, and understanding the action of electromagnetic fields on excitable tissue.